

Syntectonic fluid-flow along thrust faults: Example of the South-Pyrenean fold-and-thrust belt

Brice Lacroix^{a,*}, Anna Travé^b, Martine Buatier^c, Pierre Labaume^d, Torsten Vennemann^a, Michel Dubois^e

^a Institut des Sciences de la Terre (ISTE), Université de Lausanne, Lausanne CH-1015, Switzerland

^b Departament de Geoquímica, Petrologia i Prospecció Geològica, Universitat de Barcelona, 08028 Barcelona, Spain

^c Chrono-Environnement, UMR 6249, Université de Franche Comté-CNRS, 25000 Besançon, France

^d Géosciences Montpellier, UMR 5243, Université Montpellier 2-CNRS, 34095 Montpellier, France

^e LCGE-GEO-Environnement, Université Lille 1, 59655 Villeneuve d'Ascq Cedex, France

ARTICLE INFO

Article history:

Received 8 March 2013

Received in revised form

30 July 2013

Accepted 9 September 2013

Available online 24 September 2013

Keywords:

Thrust fault

Calcite veins

Stable isotopes

Trace elements

Fluid-flow

ABSTRACT

During compressive events, deformation in sedimentary basins is mainly accommodated by thrust faulting and related fold growth. Thrust faults are generally rooted in the basement and may act as conduits or barriers for crustal fluid flow. Most of recent studies suggest that fluid flow through such discontinuities is not apparent and depends on the structural levels of the thrust within the fold-and-thrust belt.

In order to constrain the paleofluid flow through the Jaca thrust-sheet-top basin (Paleogene southwest-Pyrenean fold-and-thrust belt) this study compares on different thrust faults located at different structural levels. The microstructures in the different fault zones studied are similar and consist of pervasive cleavage, calcite shear veins (S_{V1}), extension veins (E_{V1}) and late dilatation veins (E_{V3}). In order to constrain the nature and the source of fluids involved in fluid-rock interactions within fault zones, a geochemical approach, based on oxygen and carbon stable isotope and trace element compositions of calcite from different vein generations and host rocks was adopted. The results suggest a high complexity in the paleohydrological behaviors of thrust faults providing evidence for a fluid-flow compartmentalization within the basin. Previous studies in the southern part of the Axial Zone (North of the Jaca basin) indicates a circulation of deep metamorphic water, probably derived from the Paleozoic basement, along fault zones related to the major basement Gavarnie thrust. In contrast, in northern part of the Jaca basin, the Monte Perdido thrust fault is affected by a closed hydrological fluid system involving formation water during its activity. The Jaca and Cotiella thrust faults, in turn, both located more to the south in the basin, are characterized by a composite fluid flow system. Indeed, stable isotope and trace element compositions of the first generations of calcite veins suggest a relatively closed paleohydrological system, whereas the late calcite vein generations, which are probably associated with the late tectonic activity of the basin, support a contribution of both meteoric and marine waters. Based on these results, a schematic fluid-flow model is presented. This model allows visualization of three main fluid flow compartments along a N–S transect.

© 2013 Elsevier Ltd. All rights reserved.

1. Introduction

During the formation of a fold-and-thrust belt, organic matter trapped in sediments can reach ideal conditions to produce hydrocarbons (so-called “oil and gas window”). Thrust faults, the major structures forming thrust-and-fold belts, may act as conduits or barriers for crustal fluid flow, including hydrocarbons. Petrophysical characterization of a fault zone and reconstitution of the P–T

evolution of a fold-and-thrust belt are thus of major interests for oil companies, in order to constrain the paleohydrological characteristics of a thrust fault and to understand the fluid transport in potential reservoirs. In this context syntectonic veins, which are regarded as indicative of fluid-flow during deformation, could record essential information about the paleohydrological behavior of the fault zones (e.g. Verlaguet et al., 2011; Beaudoin et al., 2011).

The majority of previous studies focus on specific interactions between the fluids and faults (e.g. Dietrich et al., 1983; Travé et al., 1997, 1998; Badertscher et al., 2002; Wiltschko et al., 2009; Cao et al., 2010; Parry and Blamey, 2010; Lacroix et al., 2011 among

* Corresponding author. Tel.: +41 (0)21 692 43 10; fax: +41 (0)21 692 43 05.
E-mail addresses: bricelacroix@yahoo.fr, brice.lacroix@unil.ch (B. Lacroix).

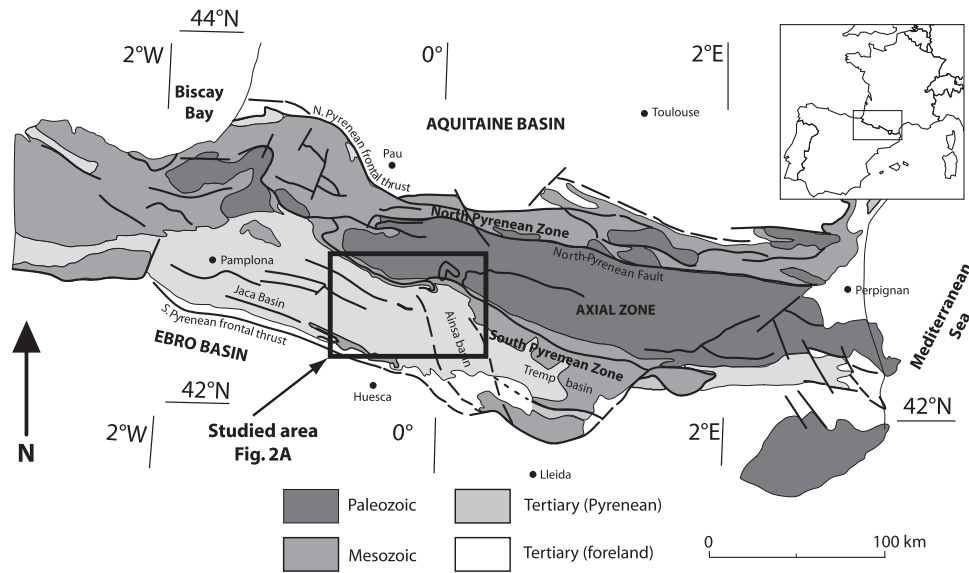


Figure 1. Structural map of the Pyrenees with the location of the study area. Modified from Lacroix et al., 2011.

others). Only a few studies (e.g. Fitz-Diaz et al., 2011) have dealt with fluid flows at the larger scale of a fold-and-thrust belt. However, at such scales, key questions are still debated, particularly with regard to the scale and the timing of fluid flow, as well as the fluid sources.

In this study we investigate fluid flow and fluid-rock interactions along the South-Pyrenean fold-and-thrust belt. This area was selected because: (1) the internal structure of the basin is well known (Teixell and Garcia-Sansegundo, 1996; Teixell, 1996; Millan Garrido et al., 2006); (2) major thrust faults outcrop in some part of the basin; (3) structures are cylindrical and plunge toward the East; (4) the emplacement of calcite-quartz veins along the thrust faults records the presence of fluid during deformation. In this area, different studies on syntectonic veins, fault zones and their relative host rocks, reveal that the hydrological behavior of thrust faults is highly complex. In the northernmost structures of the Axial Zone and its interface with the Jaca–Ainsa basin, Rye and Bradbury (1988), Henderson and McCaig (1996), and McCaig et al. (2000) demonstrated a large contribution of metamorphic fluids from the basement. In the Monte Perdido thrust fault, which developed in the silico-clastic sediments of the Eocene Hecho Group, the fluid flow was more restricted (Lacroix et al., 2011, 2012). In the Ainsa basin, Travé et al. (1997) identified the circulation of meteoric water at the front of the Cotiella thrust fault during its activity. Therefore, structural location seems to be an important factor controlling fluid–rock interactions and consequently the scale of fluid migration (Ghissetti et al., 2000, 2001).

In this research aims to decipher the structural control of thrust faults on the scale of fluid migration within part of the South-Pyrenean orogenic wedge, summarizing already published data and bringing new evidence of fluid contributions during thrusting. Two thrust faults from the Ainsa–Jaca basin, are studied here: The Jaca and Cotiella thrust faults. These two faults offer a way to understand the role of such structures in fluid migration at the basin scale since they are located at different structural positions within the orogenic prism and were developed at different times.

In order to determine the origin and nature of fluid flow along the studied thrust faults and to constrain the paleofluid system at the scale of a fault, petrography (cathodoluminescence and fluid inclusions) and geochemistry (trace elements and stable isotopes (O, C) of carbonate) were analyzed on selected syntectonic veins, fault zones and host sediments.

2. Geological setting

The Pyrenean Range corresponds to a doubly-vergent orogenic wedge formed during the convergence between the Iberian and European plates from the Late Cretaceous to the Early Miocene (e.g. Choukroune et al., 1990; Muñoz, 1992; Teixell, 1998; Beaumont et al., 2000) (Fig. 1). From the north to the south, the Pyrenean orogen is constituted of three main structural zones (Fig. 1). The North-Pyrenean Zone corresponds to a Mesozoic extensional basin system inverted and transported northward during the Pyrenean compression. The Axial Zone (Fig. 1) comprises Paleozoic rocks deformed and metamorphosed during the Hercynian orogeny, locally covered by Permian–Lower Triassic sediments. The Alpine structure of the Axial Zone corresponds to imbricated basement thrusts that pass southward to a detachment in the Triassic evaporites (Muschelkalk and Keuper) of the South-Pyrenean Zone (Fig. 2B). The South-Pyrenean Zone is affected by a south-vergent thrust-fold system and overthrusts the Ebro foreland basin along the South-Pyrenean Frontal Thrust (SPFT in Figs. 1 and 2B). The total shortening across the belt has been estimated from balanced cross sections to 165 km in the central Pyrenees (Beaumont et al., 2000) and 80 km in the western Pyrenees (Teixell, 1998), about 70% of which is accumulated in the south-verging thrust system.

The study area is located in the Jaca–Ainsa fold-and-thrust belt (Figs. 1 and 2A). The Jaca basin is separated from the Ainsa basin by the development of NNW trending Boltaña and Añisclo anticlines (Fig. 2A). Above the Triassic décollement level, the stratigraphy of the Jaca–Ainsa basin is made up of Cenomanian to Santonian platform limestones, followed by the Upper Cretaceous–Paleogene syn-orogenic succession. From bottom to top, this comprises Campanian to earliest Eocene platform carbonates, the Ypresian–Lutetian siliciclastic turbidites of the Hecho Group and Bartonian to Lower Oligocene coastal and continental deposits (e.g. Teixell, 1996).

The Jaca–Ainsa basin is affected by a set of imbricated thrusts. In the northeast part of the basin, the Hecho Group turbidites are overthrust by the Upper Cretaceous to lower Eocene carbonates of the Castillo Mayor Klippe, which corresponds to a western extension of the Cotiella thrust unit emplaced during the Early Eocene (Farrell et al., 1987; Mutti et al., 1988; Travé et al., 1997) (Fig. 2A and C). Below this unit, the Monte Perdido thrust unit, was

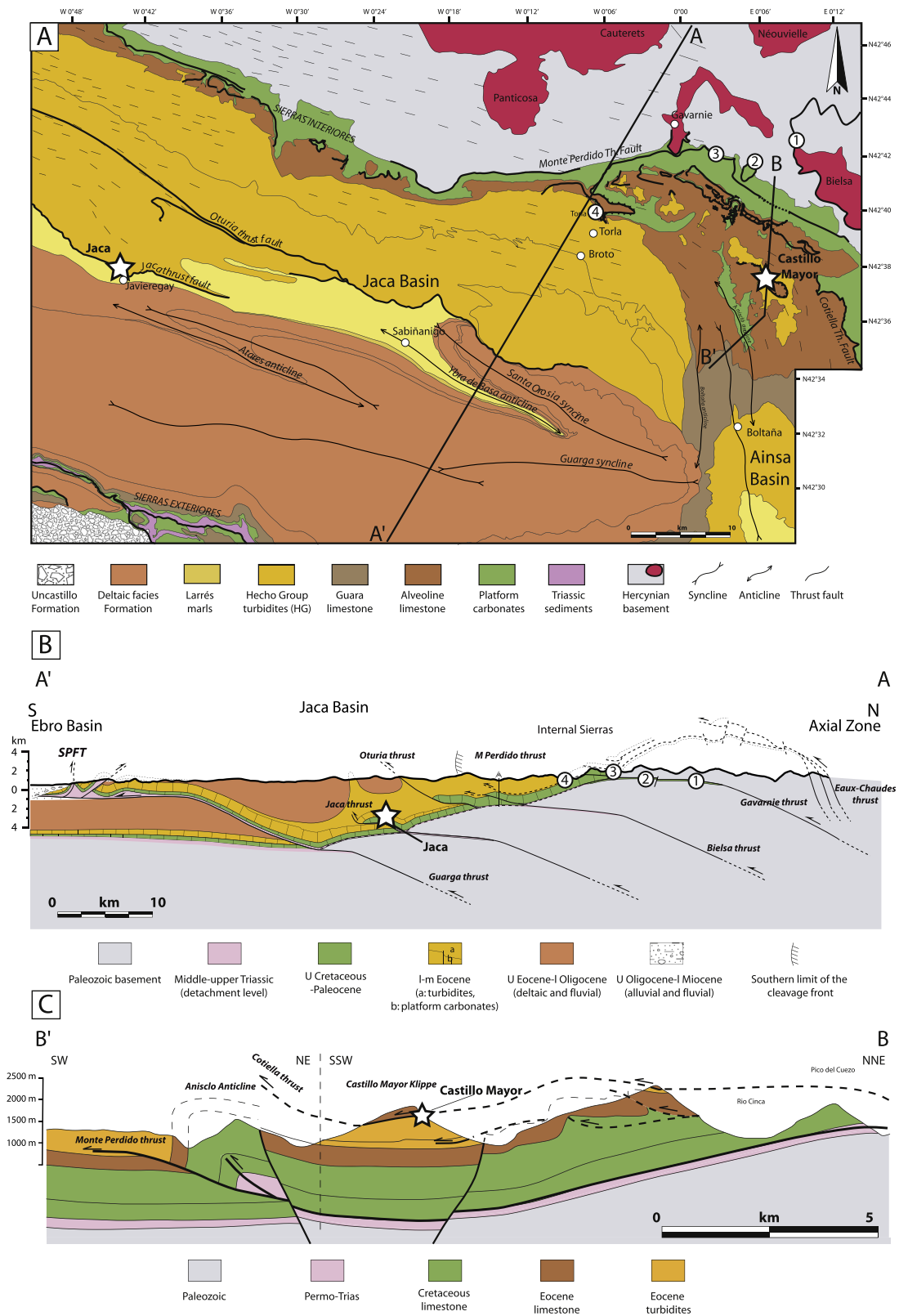


Figure 2. Detailed geological map (A) and cross sections (B and C) of the study area. **A.** Geological map compiled from geological maps published by IGME (Instituto Geológico y Minero de España) and BRGM (Bureau des recherches géologiques et minières). **B.** A–A' cross section. **C.** B–B' cross section. White stars: outcrops studied in this research. Thick black lines: thrust faults. Cleavage affecting the northern parts of the area is indicated by small black lines. Black line: Cross sections in B and C. Numbers: location of already published studies. 1: Pic de Port Vieux fault (McCaig et al., 1995); 2: Plan de Larri fault (McCaig et al., 1995); 3: Pineta thrust fault (Rye and Bradbury, 1988); 4: Monte Perdido thrust fault (Lacroix et al., 2011).

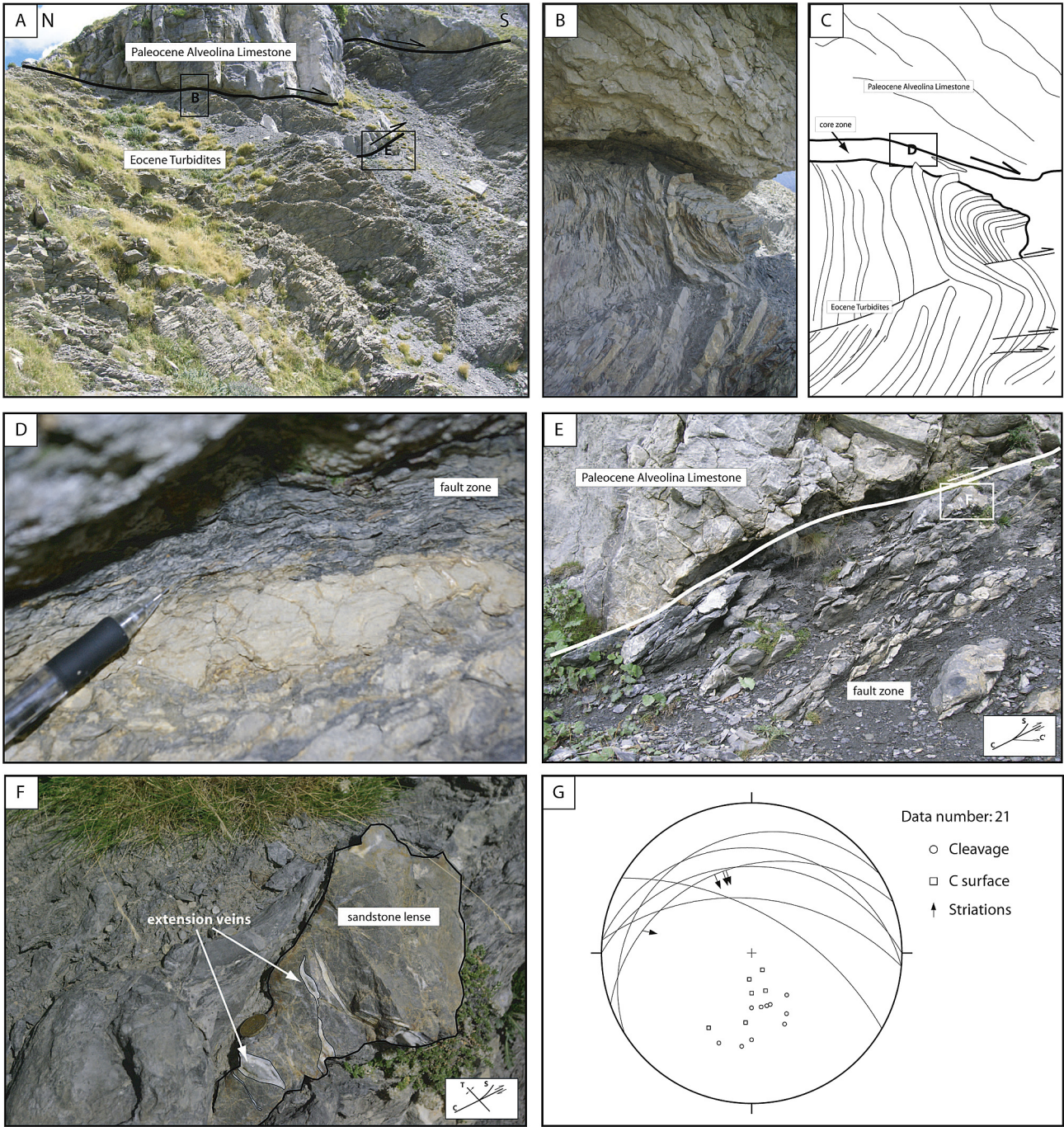


Figure 3. Field photographs and structural data illustrating the deformation in the Cotiella thrust fault (Castilló Mayor outcrop). **A.** General view of the deformed zone. **B** and **C.** View of the main contact, just below the Paleocene limestone, and its interpretation. **D.** Detail of the centimeter thick fault core zone, featuring clay-rich foliated sediments (S–C structure). **E.** Deformation zone below main fault surface (location in **A**) showing the presence of lenses from the hanging wall and footwall. **F.** Detail of a sandstone lens in the footwall deformation zone. Note the presence of extensional veins crosscutting the lens. **G.** Schmitt diagram (lower hemisphere) with plot of cleavage plane poles, shear surfaces and striations (arrows indicate the sense of displacement of the upper block); all measured structures indicate thrusting toward the south. S, cleavage; C and C', shear surfaces.

emplaced during the Middle Eocene (Lutecian–Bartonian), and is detached in the lower part of the Upper Cretaceous limestones (Fig. 2C). The front of the Monte Perdido thrust unit is marked by the development of two fault-propagation folds: the Añisclo and Boltaña anticlines (Fig. 2A and C). In the western part of the Axial Zone, the Monte Perdido fault is rooted in the Lakoura-Eau-Chaudes basement thrust system (Labaume et al., 1985; Teixell, 1996) (Fig. 2B). Later deformation during the Late Eocene and Early Oligocene caused the emplacement of the underlying Gavarnie thrust unit (Puigdefabregas, 1975; Teixell, 1996; Teixell and

García-Sanseguno, 1996) (Fig. 2B). In the medium and southern parts of the Jaca basin, the Gavarnie thrust fault is connected to two E–W trending cover thrusts: the Oturia thrust and the Jaca thrust faults (Fig. 2A and B). This latter fault, which transported the Hecho group turbidites over the Bartonian–Priabonian deltaic-continental deposits, caused the formation of the km-scale Ybra de Basa fault-propagation fold (Fig. 2A and B).

The northern part of the Jaca basin is affected by a regional pressure solution cleavage, related to the emplacement of the Monte Perdido and Gavarnie thrust units (Fig. 2A and B) (Séguret,

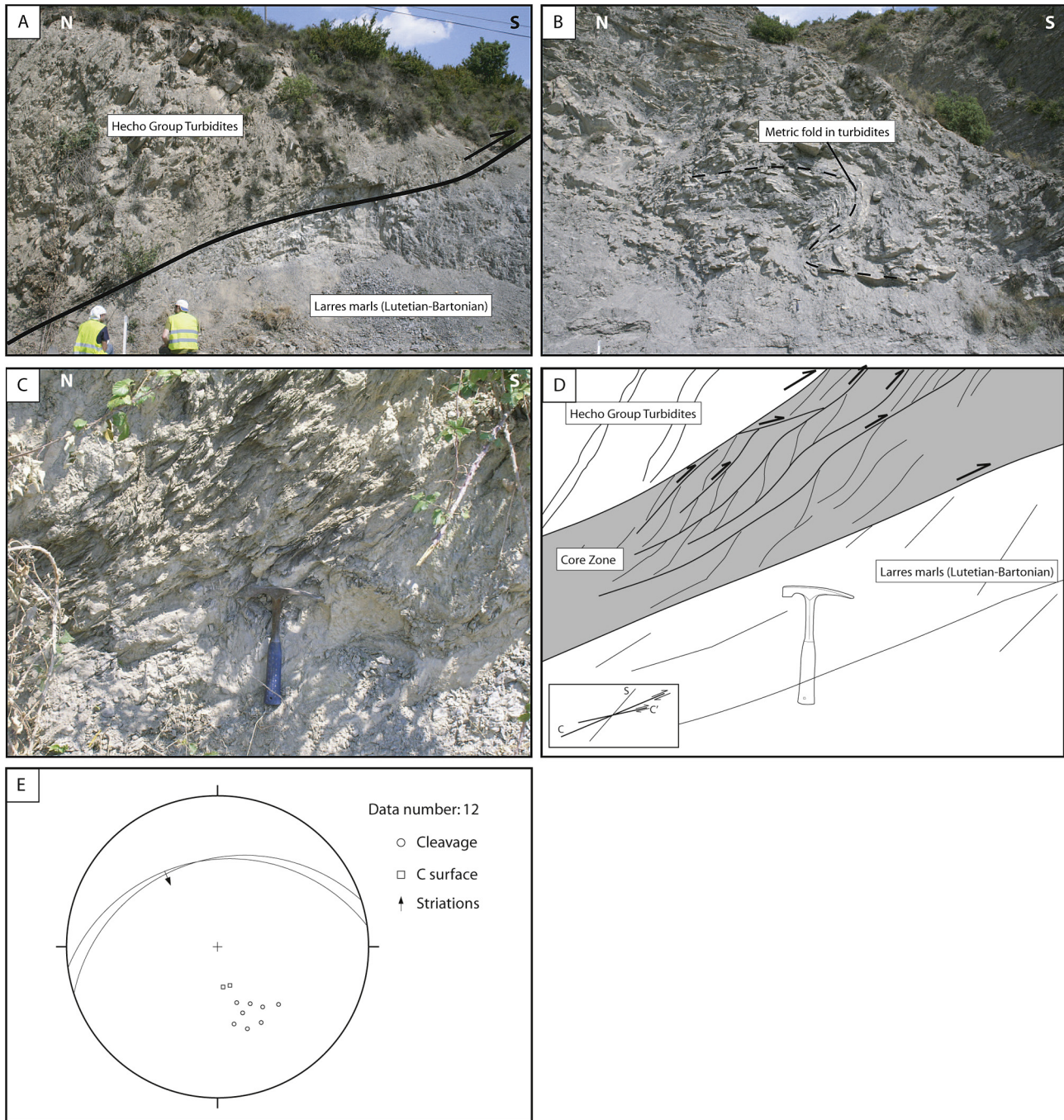


Figure 4. Field photographs and structural data illustrating the deformation in the Jaca thrust fault zone. **A.** General view of the fault zone. The hanging wall and footwall correspond to the turbidites of the Hecho Group (Lutetian) and the Larrés marls (Bartonian), respectively. **B.** Fold in turbidites from the hanging wall. **C** and **D.** Details of the core zone with cleavage (S) and shear surfaces (C and C'). **E.** Schmitt diagram (lower hemisphere) with plot of cleavage plane poles, shear plane surfaces and striation (the arrow indicates the sense of displacement of the upper block); all measured structures indicate thrusting toward the S–SE.

1972; Labaume et al., 1985; Holl and Anastasio, 1995; Teixell, 1996; Oliva-Urcia et al., 2009).

3. Outcrop descriptions

3.1. Castillo Mayor

The Castillo Mayor thrust fault is located at the front of the Cotiella thrust unit and corresponds to the westward extension of the Cotiella thrust fault studied by Travé et al. (1997, 1998 and

2007). The Castillo Mayor massif is a klippe composed of Upper Cretaceous to earliest Eocene limestones of the Cotiella unit, which overthrusts the lower part of the Hecho group turbidite succession (Figs. 2C and 3A). The main contact corresponds to a cm-thick fault core, composed of intensely deformed clay-bearing rocks (Fig. 3A–D). This major contact is underlain by a deformation zone (damage zone), which affects the footwall Hecho group turbidites (Fig. 3E). Within the fault zone, the deformation structures are characterized by closely-spaced cleavage surfaces associated with numerous anastomosing shear surface networks with a typical S–C(C')

pattern (Fig. 3E). This deformation zone corresponds to a tectonic *mélange* of competent lenses from the hanging wall (Paleocene limestone) and footwall (Hecho turbidites) (Fig. 3E). Calcite shear veins are frequent along shear surfaces and feature surface striations with an N340 mean orientation (Fig. 3G). The cleavage orientation, asymmetry of S–C structures, such as steps along shear veins striations, indicate a displacement towards the south (Fig. 3E–G). Calcite extensional veins are developed in the most competent lenses (Fig. 3F). In the hanging wall, the deformation is characterized by the development of north-dipping stylolites in the Paleocene limestone. The footwall turbidites are deformed by cm to m-scale south-verging folds and localized shear surfaces.

3.2. Jaca thrust fault

The Jaca thrust fault is located in the middle part of the Jaca basin (Fig. 2A) and accommodates the formation of the Ybra de Basa anticline (see section in Fig. 2B). In the studied outcrop, the hanging wall is made up of the Hecho Group turbidites (alternating sandstone and pelite layers), and the footwall consists of Larrés marls which is a continental facies (Fig. 4). The fault zone consists of an interval of intensely deformed clay-bearing sediments with penetrative cleavage (Fig. 4A, C and D). This latter is associated to anastomosing C–C' shear surfaces defining S–C(C') patterns (Fig. 4D). Calcite shear veins, which are often developed along shear surfaces, feature striations which are oriented to N330 (Fig. 4E). The cleavage orientation, the asymmetry of the S–C structures and the shear veins striations all indicate a displacement toward the S–SE (Fig. 4E). In the hanging wall, the Hecho Group turbidites are deformed by meter scale south-verging folds (Fig. 4B).

4. Methods

Detailed structural analysis was carried out in the field on each of the two selected outcrops. Samples of mineralized veins and deformed sediments were collected along a vertical transect through each fault zone. In the fault zone, both mineralized veins and deformed sediments were sampled. Host marls, limestones and turbidite sandstones were also collected up to about 15–30 m away from the fault zone. This distance was determined from macroscopic structural observations in the field, so that the most distal samples were not affected by significant deformation related to the major faults, but only by the background regional deformation. Optical and cathodoluminescence (CL) microscopy observations of the cements in the veins were used to document their relative chronology. The CL observations were conducted with a vacuum of 10 mTorr, a voltage of 13 kV and current of 0.5 mA.

Eighty-six microsamples of veins and host-rocks were selected from thin section observations in order to determine the carbon and oxygen stable isotopic ratio of calcite. Analyses were performed at the University of Barcelona using the standard techniques of Craig and Gordon (1965) and Claypool et al. (1980). The CO₂ was extracted from 60 ± 10 µg of the powdered carbonate samples that were reacted with 103% phosphoric acid for 2 min at 70 °C for calcites. The CO₂ was analyzed using an automated Kiel Carbonate Device attached to a Gas Source Mass Spectrometer of Thermo Electron (Finnigan) MAT-252. The results are precise to ±0.02‰ for δ¹³C and ±0.04‰ for δ¹⁸O. Results are reported in permil (‰) values relative to the Vienna PDB standard.

The trace element contents (Fe, Mg, Mn) of selected carbonate from veins were analyzed using a CAMECA model SX100 electron microprobe at the University of Montpellier equipped with five X-ray spectrometers coated thin sections. The microprobe was operated at 20 kV with a current of 10 nA and a beam diameter of 9 µm.

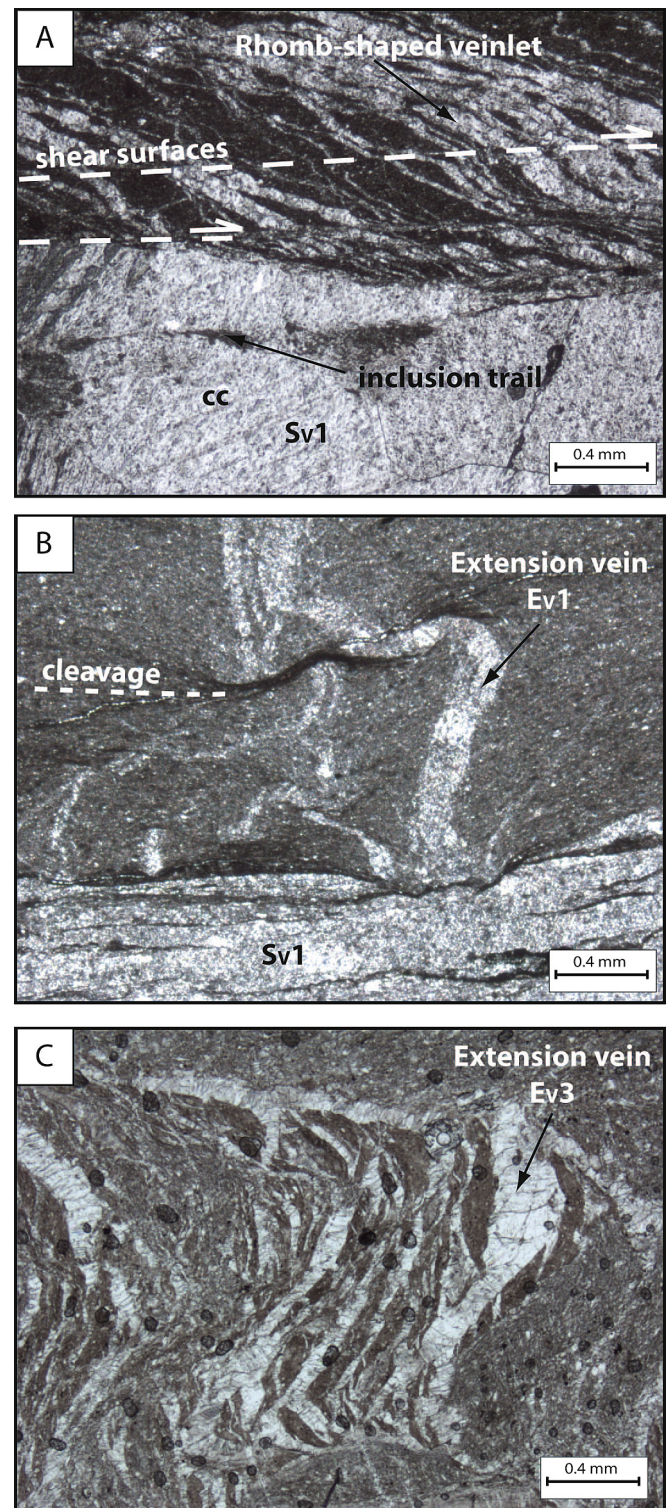


Figure 5. Optical microscope images of the different vein generations observed within the Cotiella and Jaca thrust faults. A. Example of Sv1 veins illustrating the relationship between rhomb-shaped veinlets and inclusion trails (sample from Cotiella). B. Ev1 calcite extension vein cutting cleavage at a high angle (sample from Jaca). C. Example of Ev3 dilatant veins opening pre-existing microstructures such as cleavage and shear surfaces. Note that the calcite texture is elongated showing a vein opening in all directions (sample from Jaca).

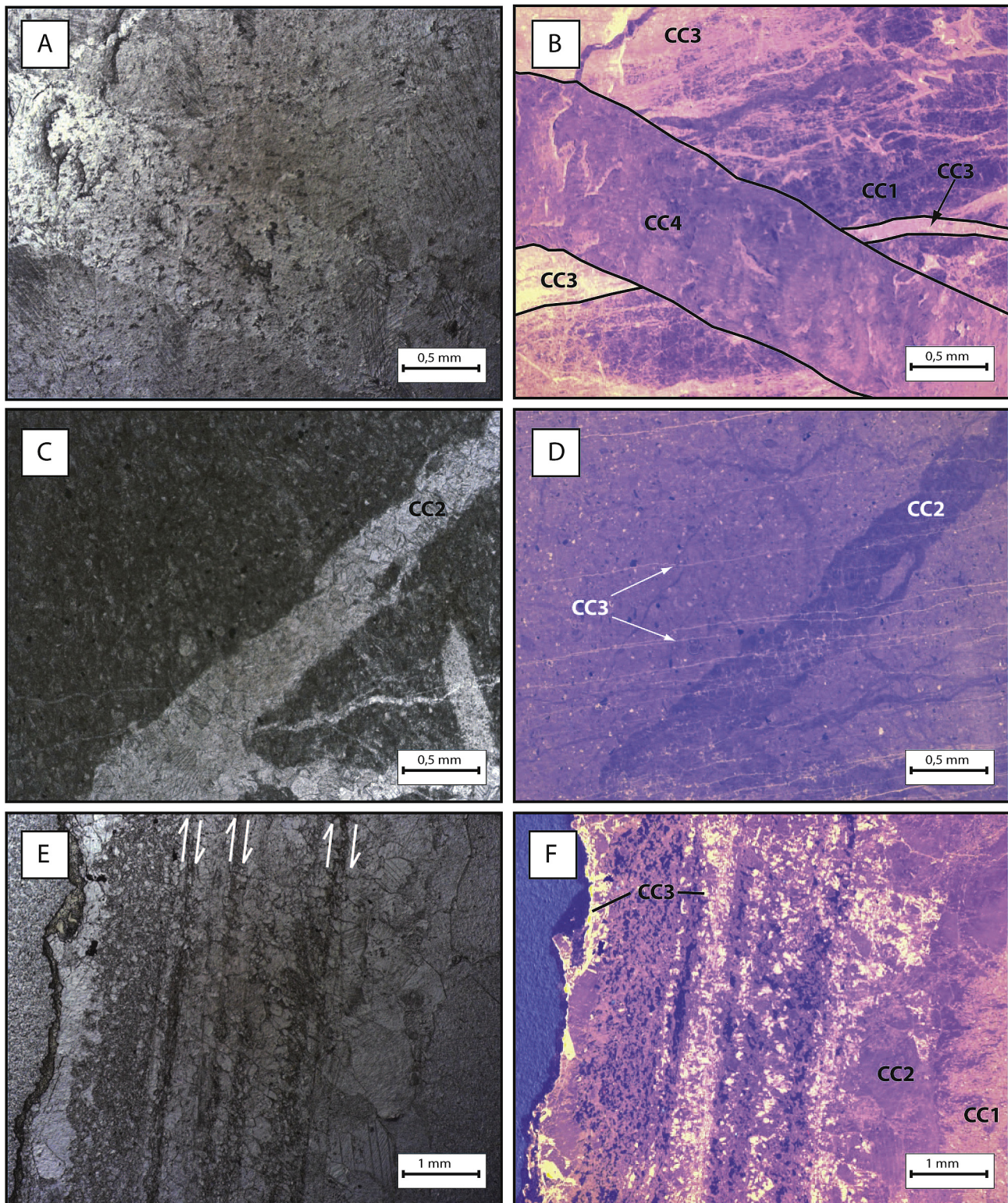


Figure 6. Petrographic and cathodoluminescence photographs illustrating the different calcite phases in the Castillo Mayor thrust fault (A and D) and the Jaca thrust fault (D and F).

The standards used were Wollastonite (Ca), Fe_2O_3 (Fe), Forsterite (Mg), Rhodochrosite (Mn) and Celestine (Sr).

Fluid inclusions were analyzed in doubly-polished wafers. Considering the relatively small grain size, sections were about $50\ \mu\text{m}$ thick and glued onto glass plates using Geoptic resin (manufactured by Brot Technologies), which can resist freezing and

moderate heating (up to $200\ ^\circ\text{C}$). Microthermometry was explored using a FLUID INC (USGS-type) heating and freezing stage. The calibration of the microthermometric stage was made using synthetic fluid inclusions (SYNFLINC; Sterner and Bodnar, 1984) including, (1) pure water (ice melting temperature = $0.0\ ^\circ\text{C}$; critical homogenization temperature = $374.1\ ^\circ\text{C}$), (2) $\text{H}_2\text{O}-\text{CO}_2$ inclusions

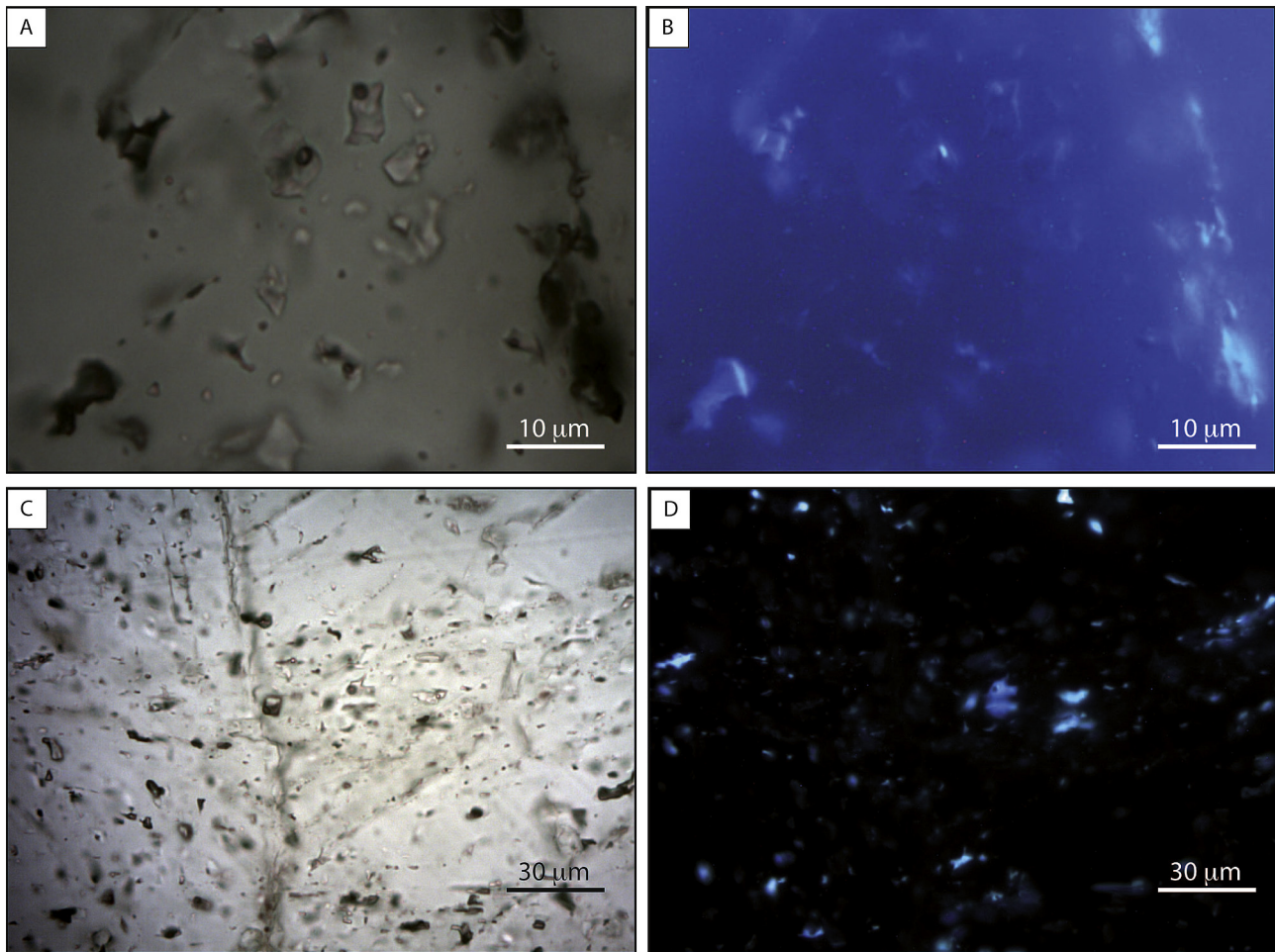


Figure 7. Photographs of fluid inclusions observed in S_V1 veins. **A.** Sample from Castillo Mayor (S_V1 vein) showing water and methane inclusions in transmitted light. **B.** Same inclusions observed with Ultra-violet (UV) light showing no fluorescence. **C and D.** Hydrocarbon inclusions from the Jaca fault showing gas-rich inclusions observed in transmitted light (**C**) and (**D**) with UV light showing gas-rich inclusions.

(CO_2 melting temperature = -56.6 °C; hydrate melting temperature = $+10.0$ °C) and (3) H_2O – NaCl inclusions (eutectic temperature = -21.2 °C). Accuracy is ± 0.1 °C at temperature between -56.6 and $+25$ °C and up to about ± 1 °C at $+400$ °C. Inclusions were studied respecting the concept of Fluid Inclusion Assemblage (FIA; Goldstein and Reynolds, 1994; Goldstein, 2003). Each FIA is composed of a few inclusions (generally about 10, but sometimes less) taken to be representative of the same trapping event.

Raman microspectrometry was performed at the Géosystèmes Laboratory (University of Lille 1). Raman spectra were recorded with a LabRam HR800 Jobin-Yvon™ microspectrometer equipped with 1800 g/mm gratings and using 532.28 nm (green) laser excitation. Acquisition timespan varied from 20 to 60 s during three accumulating cycles. Vapor bubbles were investigated in order to evaluate the presence of volatile species (CH_4 , CO_2 , N_2 , H_2S). Analytical problems were encountered due to the bubble mobility at room temperature.

5. Petrographic study

5.1. Microstructures

For both outcrops, the microstructures present in the fault zone are similar and consist of pervasive pressure-solution cleavage,

calcite shear veins and extension veins (respectively S_V1 and E_V1). A late generation of dilation veins, referred to as E_V3 , is also observed in both thrust faults. Nevertheless, their morphologies are different (see below). The typology defined by Lacroix et al. (2011) was adopted, where all the microstructures are discussed in detail and are briefly summarized below.

5.1.1. Calcite shear veins (S_V1)

The calcite shear veins correspond to cm-thick tabular bodies with metric to decametric lateral extensions. Microscopically, they consist of layered veins opened by a combination of incremental Mode II shear surfaces and Mode I openings (Lacroix et al., 2013). Each layer consists of millimeter thick sheets, bounded by two inclusion trails and formed by the lateral succession of millimeter-sized rhomb-shaped veinlets (Fig. 5A). The inclusion trails correspond to shear surfaces while the rhomb-shaped veinlets correspond to mode I extensional fractures normal to cleavage surfaces (Fig. 5A). This generation of veins is contemporaneous with the main thrust fault emplacement.

5.1.2. Calcite extension veins (E_V1)

Calcite extension veins correspond to thin veins subnormal to the pressure solution cleavage (Fig. 5B). They are filled with blocky to elongated calcite crystals, perpendicular to the vein boundaries, supporting a mode I opening. Crosscutting relationships show that

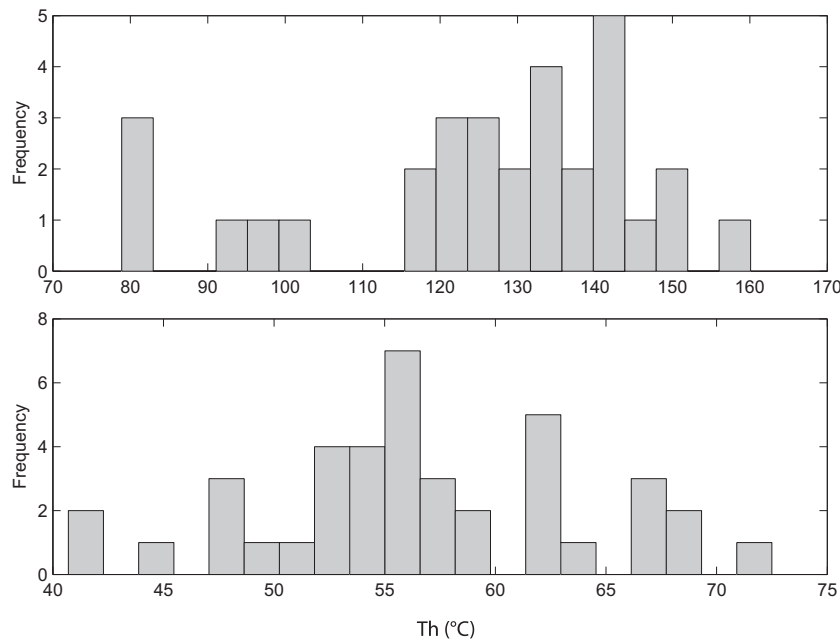


Figure 8. Frequency plots of measured homogenization temperatures (T_h) of fluid inclusions present in S_{V1} veins from the Castillo Mayor (A) and Jaca (B) fault zones.

these veins were formed contemporaneously with the calcite shear veins.

5.1.3. Late calcite extension veins (E_{V3})

Late calcite extension veins are observed in both the Jaca and Cotiella fault zones. In the Castillo Mayor thrust fault the E_{V3} veins correspond to thin extensional veins crosscutting the most competent clasts and tabular S_{V1} veins (e.g. Fig. 6A and B). In the Jaca thrust fault, the E_{V3} veins correspond to irregular vein networks filled with blocky to elongated calcite crystals (Fig. 5C). The E_{V3} veins usually follow pre-existing microstructures such as cleavage and shear surfaces. When such veins present an elongated texture, the calcite crystals are perpendicular to the vein boundaries, suggesting that they initially opened in different directions (Fig. 5C).

5.2. Cathodoluminescence

5.2.1. Castillo Mayor thrust fault

Cathodoluminescence observations reveal four calcite cement phases (Fig. 6A–D). The calcite phases referred to as CC1 and CC2 constitute the majority of the S_{V1} and E_{V1} vein cements. These calcite cements are characterized by a dark blue (in the web version) luminescence (Fig. 6B). CL observations reveal that the S_{V1} veins and host sediment are cut by late extension fractures (referred to as CC3 and CC4), which are not necessarily visible with traditional optical microscopy. CC3 is characterized by a very bright yellow (in the web version) CL (Fig. 6B and D). The later calcite phase (CC4), which fills mm-thick fractures, is observed in the S_{V1} veins and produces a CL similar to CC1 and CC2 (Fig. 6D).

5.2.2. Jaca thrust fault

In the S_{V1} shear veins from the Jaca thrust fault, CL observations reveal three calcite phases, referred to as CC1, CC2 and CC3 (Fig. 6E and F). The CC1 phase is characterized by brown-orange CL and constitutes up to 70% of the vein filling. The CC2 phase corresponds to a dark blue (in the web version) calcite CL. The limit between the CC1 and CC2 calcite cements is diffuse. The CC3 phase is only present at the proximity of shear surfaces within the shear veins,

and is characterized by bright yellow (in the web version) CL. The spatial relationship between the CC3 phase and shear attests to the fact that CC3 corresponds to a late calcite cement phase in the S_{V1} veins.

5.3. Fluid inclusion analyses

5.3.1. Analytical results

Fluid inclusions from the S_{V1} , E_{V1} and E_{V3} (only for Jaca) veins from both outcrops were studied using an optical microscope. In both fault zones S_{V1} veins, which are considered to be syntectonic, contain mostly primary and pseudo-secondary two-phase inclusions, including a vapor bubble and a liquid phase. Fluid Inclusion Assemblages generally comprise 2–10 inclusions, rarely more.

In the Castillo Mayor fault, fluid inclusions are mainly pseudo-secondary on the basis of Roeder's criteria (Roeder, 1984). The inclusions morphologies are irregular (immature) (Fig. 7A) and sizes range from 2 to 10 μm . Vapor bubbles generally move rapidly at room temperature. No fluorescence of the liquid phase was observed under Ultra-Violet (UV) light (Fig. 7B).

In the Jaca fault, the S_{V1} shear veins and late extensive veins (E_{V3}) contain inclusions with sizes ranging from 2 to 5 μm . The inclusion morphologies are mostly cubic to rectangular (Fig. 7C). Inclusions were classified as primary on the basis of criteria after Roeder (1984). The liquid phase exhibits green–blue fluorescence when exposed to a UV-source (Fig. 7D). This indicates that the liquid phase is composed of high API-density hydrocarbons (Bodnar, 1990), i.e. light hydrocarbons. FIA observed in the late extensive veins (E_{V3}) correspond to 5–10 mm-cubic single liquid phase inclusions, suggesting trapping temperatures lower than 70 °C (Goldstein, 1986).

Inclusions were initially heated in order to measure homogenization temperatures (T_h). In samples from the Castillo Mayor, T_h values are scattered and range from 136 to 201 °C, although the majority of the data lie in the range 115–155 °C (Fig. 8A). For samples from Jaca, T_h values form a well-defined distribution with a peak at 56 °C (Fig. 8B). Unfortunately, low temperature analyses (cryometry) rarely show phase transitions that are easily interpretable.

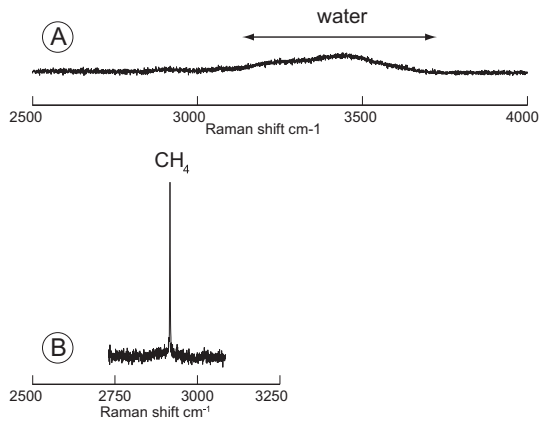


Figure 9. Raman spectra of components identified in fluid inclusions from Castillo Mayor veins. **A.** Raman spectrum of the liquid phase, showing the water band at 3100–3600 cm^{-1} . **B.** Raman spectrum obtained on the vapor bubble, showing a tight peak at about 2910 cm^{-1} , corresponding to methane.

Raman spectroscopy was applied to both the liquid and vapor bubbles. In sample from Castillo Mayor, the vapor bubble analyses indicate the presence of a tight peak at about 2910 cm^{-1} , corresponding to methane (Fig. 9A) (Frezzotti et al., 2012). The characteristic band of water (2900–3600 cm^{-1}) was also recorder from the liquid phase of the inclusions (Fig. 9B) (Frezzotti et al., 2012). In samples from Jaca, the strong fluorescence did not allow any Raman analysis of the liquid phase; analyses of the vapor bubble were also unsuccessful because of the rapid bubble movement.

5.3.2. Interpretation of fluid inclusion data

Fluid inclusion characterization techniques reveal that inclusions from both faults are composed of hydrocarbons. The trapping temperatures of the inclusions can be estimated using T_h . In Castillo Mayor, the large range of T_h values probably results from heterogeneous trapping temperatures. Inclusions are composed of a mixture of water and methane; this indicates that water was probably saturated with respect to methane (Goldstein and Reynolds, 1994). If we assume that the large T_h range also results from the stretching of inclusions, the lower T_h can be used as the true trapping temperature (about 115 °C).

In the Jaca fault, T_h data are centered around a 56 °C modal peak, which corresponds with the minimal trapping temperature. A pressure correction of about 20 °C can be estimated using a classical

geothermal gradient of 30 °C/km, therefore a mean T_h value of 76 °C can be used as the trapping temperature.

Fractures along both of the faults studied have acted as conduits for hydrocarbons from different reservoirs. In sample from Castillo Mayor, fluids of about 115 °C probably originated from a deep methane reservoir, whereas in samples from the Jaca fault, more complex hydrocarbons with a temperature of about 76 °C probably have a more local origin.

6. Geochemistry

6.1. Trace element content of calcite veins (Mn, Mg and Fe)

According to Boles et al. (2004), the trace-element composition of carbonate cements in veins indicates the type of mineralizing fluid. Microprobe analyses indicate that the Mg, Mn and Fe contents of carbonates display large variations (Fig. 10).

6.1.1. Castillo Mayor thrust fault

In the Cotiella thrust fault, the compositions of calcite phases CC1, CC2 and CC4 are similar (Fig. 10A). They are characterized by low-Mn and high-Mg and Fe contents. This composition indicates precipitation from formation water (Travé et al., 1997). In contrast, the high-Mg content in the CC3 calcite phase supports precipitation from marine water (Dromgoole and Walter, 1990; Wogelius et al., 1997; Cao et al., 2010).

6.1.2. Jaca thrust fault

In the Jaca thrust fault, the calcite phases CC1 and CC2 are very similar; both have low-Mn content and intermediate Mg and Fe content (Fig. 10B). These compositions indicate that calcite precipitated from formation water (Travé et al., 1997). The composition of the CC3 calcite phase is characterized by very low Fe content, suggesting precipitation from continental meteoric water (Boles et al., 2004; Cao et al., 2010).

6.2. Stable isotope compositions

For both faults studied, oxygen and carbon stable isotope analyses have been made on bulk rocks (host and deformed sediments) and on calcite cements from the Sv1, Ev1, and Ev3 veins. Results are reported in Figure 11 and Table 1. Unfortunately the different calcite cements revealed by CL petrography were too small to be analyzed.

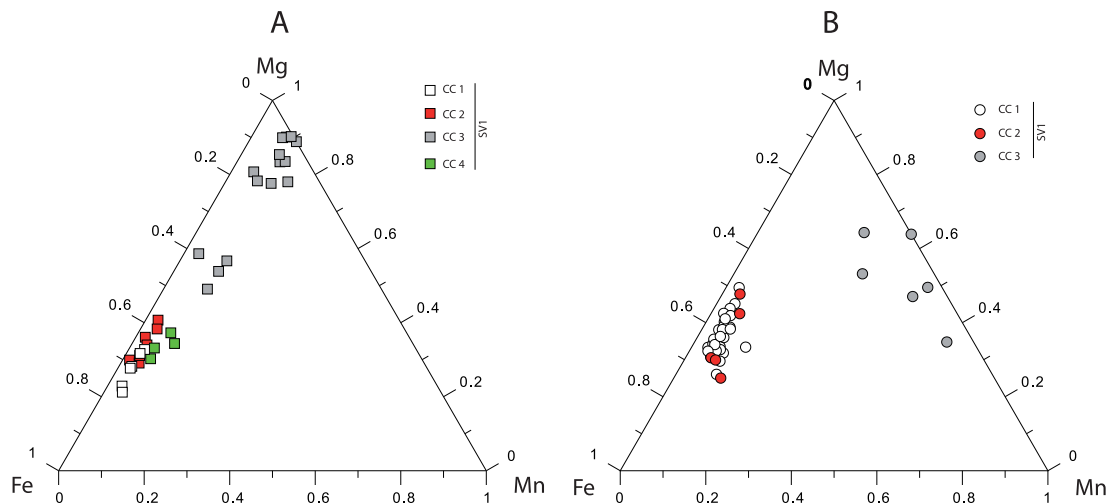


Figure 10. Ternary plot of the calcite trace element content (Fe–Mn–Mg) of the different calcite phases observed in the Cotiella (A) and the Jaca (B) thrust faults.

The isotopic analyses presented in this section thus correspond to mixtures of the different cements.

6.2.1. Castillo Mayor thrust fault

The isotopic values of calcites from the hanging wall limestone vary from -8.5 to -7.5 ‰ VPDB for $\delta^{18}\text{O}$ and from $+0.4$ to $+1.2$ ‰ VPDB for $\delta^{13}\text{C}$ (Fig. 11A). These values are similar to those reported for the same lithology from the hanging wall of the Monte Perdido thrust fault, in the northern part of the Jaca basin (Lacroix et al., 2011). The Early Eocene turbidites from the footwall have different isotopic compositions, with $\delta^{18}\text{O}$ and $\delta^{13}\text{C}$ ranging from -7.4 to -6.1 ‰ VPDB and from -2.1 to -1.0 ‰ VPDB, respectively (Fig. 11A).

In the core zone, the $\delta^{13}\text{C}$ and $\delta^{18}\text{O}$ values of deformed sediments, S_{V1} and E_{V1} veins are intermediate between those of the respective hanging wall and footwall. Such compositions suggest that fluid-rock ratios were low in the fault zone such that the mineralized fluid was largely buffered by the host carbonate. The oxygen isotopic compositions of the fluid from which the S_{V1} calcite veins precipitated were determined using the Zheng (1999) calibration and temperatures estimated by fluid inclusion microthermometry (mean value of 140 °C). The calculated $\delta^{18}\text{O}$ values of the fluid ranges from $+10.0$ ‰ to 11.3 ‰ VSMOW. These values are consistent with formation water (Longstaffe, 1987).

6.2.2. Jaca thrust fault

Host and deformed sediments from this fault yield very similar $\delta^{18}\text{O}$ and $\delta^{13}\text{C}$ values, ranging from -6.4 to -5.1 ‰ VPDB and from -1.6 to -0.4 ‰ VPDB, respectively (Fig. 11B). In the S_{V1} veins, the $\delta^{13}\text{C}$ values are very close to those from host sediments whereas the $\delta^{18}\text{O}$ values are slightly lower ranging from -6.7 to -6.6 ‰ VPDB (Fig. 11B). Calcite from the E_{V3} veins yields similar $\delta^{13}\text{C}$ values, and the lowest $\delta^{18}\text{O}$ values which range from -7.8 to -7.1 ‰ VPDB (Fig. 11B).

The similarity of the $\delta^{13}\text{C}$ values between the veins and host-deformed sediments indicates that the fluid was partially buffered by the C-isotope compositions of the deformed host sediments. The oxygen depletion in the S_{V1} and E_{V3} veins (where E_{V3} is more depleted than S_{V1}) is interpreted to reflect mineralization of calcite from an external fluid (meteoric or metamorphic water) and/or a temperature effect. Considering the 50 – 64 °C temperature range estimated for the fluid inclusions in the S_{V1} veins and using the calcite-water fractionation curve from Zheng (1999), the calculated fluid composition varies from -2.1

to -0.9 ‰ VSMOW for $\delta^{18}\text{O}$. Such fluid compositions suggest that calcite from S_{V1} precipitated from meteoric water or from a mixture of formation and meteoric waters. The E_{V3} veins formed at temperature lower than 70 °C and require even more $\delta^{18}\text{O}$ -depleted mineralizing fluid composition typical of meteoric water.

7. Discussion

7.1. Fluid history of Cotiella and Jaca thrust faults

Both faults studied are located at the front of different thrust units formed at different periods during the Pyrenean orogeny. Consequently their histories of fluid evolution are different, as described below.

7.1.1. Initial fluid system during thrusting

For both faults studied, petrographical and geochemical data attest to the formation of different calcite cementation phases during thrust fault activity (CC1, CC2 and CC4, with CC4 only observed in the Castillo Mayor fault). The previous calcite phases display high Mg and Fe and low Mn contents (Fig. 10) suggesting that they precipitated from local formation water. In the Cotiella fault, stable isotope compositions suggest that the calcite cements in the veins are in isotopic equilibrium with their host rocks. This indicates that the deformation inside the fault zone was associated with low fluid-rock ratios, where the fluid geochemistry was largely buffered by the carbonate fraction of the host sediments. Moreover, the calculated $\delta^{18}\text{O}$ values of the mineralizing fluid are consistent with local formation water. This type of fluid could be present in the pore spaces of sediments within which it was re-equilibrated during burial diagenesis (Longstaffe, 1987; Longstaffe et al., 2003; Sharp, 2009).

For the Jaca fault, the fluid history is slightly different. Although the first calcite cementation phases (CC1 and CC2) also display high-Mg and Fe contents (Fig. 10), suggesting precipitation from local formation water, the oxygen isotopic composition of calcite from S_{V1} veins coupled with microthermometric data indicate to the main fluid involved in the system being a poorly evolved formation water, probably mixed with meteoric water, hence with a fluid/rock ratio that was somewhat higher compared to the Cotiella fault. Furthermore, light hydrocarbons trapped at about 76 °C in inclusions from the Jaca fault probably originated from a local hydrocarbon reservoir. Therefore, during the Jaca

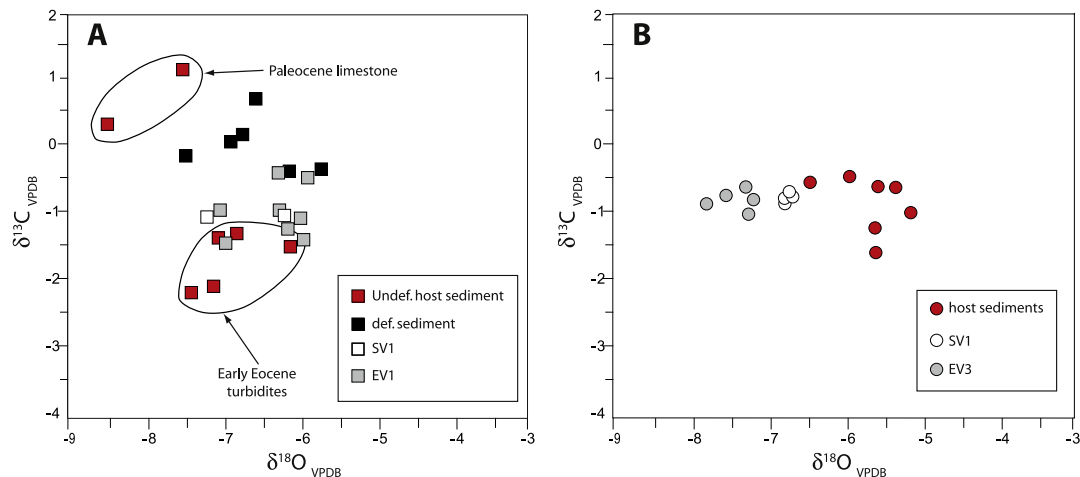


Figure 11. Isotopic compositions ($\delta^{18}\text{O}$ and $\delta^{13}\text{C}$, ‰) of calcite samples from veins and host sediments (fault zone, hanging wall and footwall) from the Cotiella (A) and Jaca (B) thrust faults.

Table 1
Oxygen and carbon isotopic data from Castillo Mayor and Jaca fault zones.

Samples	$\delta^{13}\text{C}$ PDB	$\delta^{18}\text{O}$ PDB	$\delta^{18}\text{O}$ SMOW	Description	Location	
Jaca	Ja03 – 1	–1.0	–5.1	25.3	Foliated sediment	Host sediment
Jaca	Ja03 – 4	–1.2	–5.6	24.8	Foliated sediment	Host sediment
Jaca	Ja04 – 4	–0.6	–5.3	25.1	Foliated sediment	Host sediment
Jaca	Ja05 – 1	–1.5	–5.6	24.8	Turbidite marl	Host sediment
Jaca	Ja06 – 1	–0.4	–5.9	24.5	Foliated sediment	Host sediment
Jaca	Ja08 – 4	–0.5	–6.4	23.9	Foliated sediment	Host sediment
Jaca	Ja09 – 2	–0.6	–5.5	24.8	Foliated sediment	Host sediment
Jaca	Ja07 – 1	–0.7	–6.7	23.6	S _v 1	Fault zone
Jaca	Ja08 – 2	–0.6	–6.7	23.7	S _v 1	Fault zone
Jaca	Ja09 – 1	–0.7	–6.6	23.7	S _v 1	Fault zone
Jaca	Ja04 – 2	–0.8	–6.7	23.6	S _v 1	Fault zone
Jaca	Ja04 – 1	–1.0	–7.2	23.1	E _v 3	Fault zone
Jaca	Ja08 – 1	–0.7	–7.1	23.2	E _v 3	Fault zone
Jaca	Ja08 – 3	–0.8	–7.8	22.5	E _v 3	Fault zone
Jaca	Ja08 – 3	–0.6	–7.2	23.1	E _v 3	Fault zone
Jaca	Ja08 – 3	–0.7	–7.5	22.8	E _v 3	Fault zone
Castillo Mayor	CM01	0.4	–8.5	21.8	Limestone	Hanging wall
Castillo Mayor	LCM01 – 1	1.2	–7.5	22.8	Limestone	Hanging wall
Castillo Mayor	LCM02 – 3	–0.1	–7.5	22.9	Foliated sediment	Fault zone
Castillo Mayor	LCM02 – 4	0.2	–6.7	23.6	Foliated sediment	Fault zone
Castillo Mayor	LCM04 – 1	–1.3	–6.8	23.5	Foliated sediment	Fault zone
Castillo Mayor	LCM05 – 1	0.1	–6.9	23.5	Foliated sediment	Fault zone
Castillo Mayor	LCM05 – 5	–0.3	–5.7	24.7	Foliated sediment	Fault zone
Castillo Mayor	LCM06 – 3	–0.3	–6.1	24.3	Foliated sediment	Fault zone
Castillo Mayor	LCM08 – 1	0.7	–6.5	23.8	Foliated sediment	Fault zone
Castillo Mayor	CM 06	–2.1	–7.4	22.9	Turbidite marl	Footwall
Castillo Mayor	CM 06	–2.1	–7.1	23.2	Turbidite marl	Footwall
Castillo Mayor	CM07	–1.5	–6.1	24.2	Turbidite marl	Footwall
Castillo Mayor	LCM10 – 1	–1.3	–7.0	23.3	Turbidite marl	Footwall
Castillo Mayor	LCM02 – 2	–1.0	–6.2	24.2	S _v 1	Fault zone
Castillo Mayor	LCM05 – 2	–1.0	–7.2	23.1	S _v 1	Fault zone
Castillo Mayor	LCM05 – 3	–1.4	–6.9	23.4	E _v 1	Fault zone
Castillo Mayor	LCM05 – 4	–0.9	–6.2	24.1	E _v 1	Fault zone
Castillo Mayor	LCM06 – 1	–1.3	–5.9	24.4	E _v 1	Fault zone
Castillo Mayor	LCM06 – 2	–1.0	–6.0	24.4	E _v 1	Fault zone
Castillo Mayor	LCM08 – 2	–0.4	–5.9	24.5	E _v 1	Fault zone
Castillo Mayor	LCM08 – 3	–0.9	–7.0	23.3	E _v 1	Fault zone
Castillo Mayor	LCM08 – 4	–0.3	–6.2	24.1	E _v 1	Fault zone
Castillo Mayor	LCM02 – 1	–1.2	–6.1	24.2	E _v 1	Fault zone

fault activity, the fault zone probably acted as a drain where mixtures of meteoric water, local hydrocarbons and formation water occurred.

7.1.2. Late opening of the fluid system

In both fault zones studied, the latest deformation event is associated with an opening of the fluid-system which clearly involves surface waters. Indeed, in the Jaca thrust fault, the CC3 calcite cement phase from the S_v1 veins with low Fe contents probably precipitated from meteoric, continental water. Furthermore, the fluid from which the E_v3 calcite was precipitated is characterized by a lower $\delta^{18}\text{O}$ values typical for meteoric waters. In contrast, in the Castillo Mayor thrust fault, trace-element contents suggest that the CC3 calcite phase from the S_v1 veins precipitated from marine water, in agreement with the conclusions made by Travé et al. (1998).

For both faults studied, the transition from a local fluid source, involving formation water and related hydrocarbons, to an external surficial fluid implies the opening of the hydrological fault system during deformation. This implies that during late deformation the fault became connected to the topographic surface. This external fluid flow episode is associated with the development of late extensive calcite veins (E_v3) and a late calcite cementation phases (CC3) in the S_v1 shear veins of the Jaca thrust fault, whereas in the Castillo Mayor fault it is only recognized in the late extensional phases.

7.1.3. Consistency with the regional geology

The fluid evolution along both faults is in agreement with the geological history of the Ainsa-Jaca basin. In the Castillo Mayor thrust fault, the late opening of the hydrological system is associated with the precipitation of calcite from a marine fluid. Such a fluid contribution is expected since the Cotiella thrust fault was formed under submarine conditions during deposition of the lower part of the Eocene Hecho Group turbidites (Farrell et al., 1987; Mutti et al., 1988; Travé et al., 1997; Hoareau et al., 2009). The Cotiella thrust fault was connected to the seabottom during this activity; this is especially the case for the Castillo Mayor klippe, which is located at the front of the Cotiella nappe. Travé et al. (1997, 1998) studied different fault zones and related folds located at the front of the Cotiella unit. They highlighted the participation of formation waters to marine waters during the early deformation stage and, subsequently, the influence of meteoric water derived from the emerged part of the belt.

For the Jaca fault, which consists of a branch of the Gavarnie thrust fault, syntectonic unconformities along the Yebra de Basa anticline (Fig. 2A and B) allow the activity of the Jaca thrust fault to be dated as ranging from the Priabonian to the Early Oligocene period during which the Jaca basin fill changed from marine (deltaic) facies to continental (fluvial and alluvial-fluvial) facies (Puigdefabregas, 1975; Teixell and Garcia-Sansegundo, 1996; Jolivet et al., 2007; Meresse, 2010). During this period, the fault zone

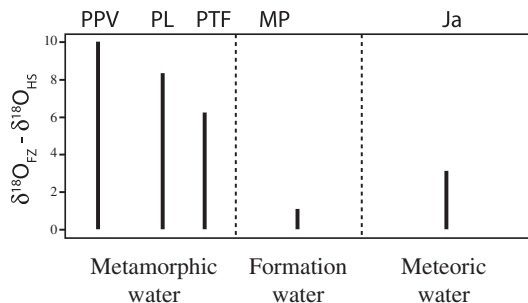


Figure 12. Synthesis of oxygen isotopic shifts between the different fault zones (FZ) from the south Pyrenean orogenic wedge and their host sediments (HS). Three different zones are distinguished by function of the contributing fluid origin (Metamorphic water, formation water and Meteoric/Marine water). PPV: Pic de Port Vieux fault (McCaig et al., 1995); PL : Plan de Larri fault (McCaig et al., 1995); PTF: Pineta thrust fault (Rye and Bradbury, 1988); MP: Monte Perdido thrust fault (Lacroix et al., 2011); Co: Cotiella thrust fault (this study); Ja: Jaca thrust fault (this study).

was probably connected to the surface above sea-level, allowing the infiltration of meteoric fluids.

7.2. Regional fluid scale transport along the Jaca basin

Different studies provide data on fluid-rock interactions and fluid transport along specific thrust faults from the South-Pyrenean wedge (e.g. Rye and Bradbury, 1988; McCaig et al., 1995, 2000; Henderson and McCaig, 1996; Lacroix et al., 2011). From these studies, also based on oxygen isotopic compositions, different assumptions about fluid flow along the Jaca basin can be made. A synthesis of the oxygen isotopic compositional differences between the host rocks and the fault zones from these different studies are presented in Figure 12. In the axial zone, McCaig et al. (1995) studied a branch of the Gavarnie thrust fault. Their isotopic data (Fig. 12) revealed a large δ¹⁸O shift of about 12‰ in deformed sediments and calcite veins compared to the protolith (Fig. 12). They interpreted this shift as the re-equilibration of the oxygen isotopic compositions of deformed rocks with a deeper metamorphic fluid, and assumed the possibility of a thermal anomaly in the thrust fault. In their most recent study, based on fluid inclusion geochemistry, McCaig et al. (2000) demonstrated the contribution of fluid buffered by hypersaline Triassic levels before transport.

Further to the south, Rye and Bradbury (1988) studied the Pineta thrust fault, a branch of the Monte Perdido thrust fault affecting Cretaceous limestone. Although less important than suggested by the McCaig’s study, they also reported an oxygen isotope shift of about 6‰ (Fig. 12) which they interpreted as the effect of a deeper metamorphic fluid circulation during deformation.

In the northern part of the Jaca basin (Sierras Interiores), Lacroix et al. (2011) provided oxygen isotopic values of calcite veins and deformed sediments from the Monte Perdido thrust faults. The high δ¹⁸O values of calcite veins, deformed sediments and host sediments (Fig. 12) support a closed fluid system during deformation.

In the present study, results obtained on the Jaca thrust fault provide new data on the southern part of the Jaca basin. Stable isotope analyses highlight a shift in oxygen isotope values between fault zones (provided by both Sv1 and Ev3 calcite veins) and host sediments (Fig. 12). As demonstrated above, this shift could be related to the infiltration of low temperature meteoric water during late thrust fault activity.

The results presented above and those already published on fluid flow along thrust faults from the South Pyrenean fold-and-thrust belt are compiled in a balanced cross section in Figure 13. This leads to a schematic visualization of the fluid flow through the Jaca basin. Note that the different locations are projected on the same cross section that is considered to be representative. Given the difficulty of incorporating the Cotiella thrust fault, which is located in the Ainsa basin, it was decided to integrate only data from the Jaca thrust fault, which is structurally more consistent with the reference cross section. The model allows visualization of three different fluid-flow compartments along the NS transect in the Pyrenean wedge.

In the north, thrust fault roots (Gavarnie and Mont Perdido) from the axial zone affecting the first levels of the sedimentary series, act as conduits for metamorphic fluids (Fig. 13). This could be explained by the rheological behavior of limestone and metamorphic and crystalline basement rocks during fracture formation. Such rocks develop high fracture density and high permeability during faulting, which would allow larger amounts of fluid to be transported from a deeper source.

In the Jaca basin, Lacroix et al. (2011) highlighted the contribution of formation water in the Monte Perdido thrust fault during its activity (Fig. 13) suggesting a hydrologically closed fluid system.

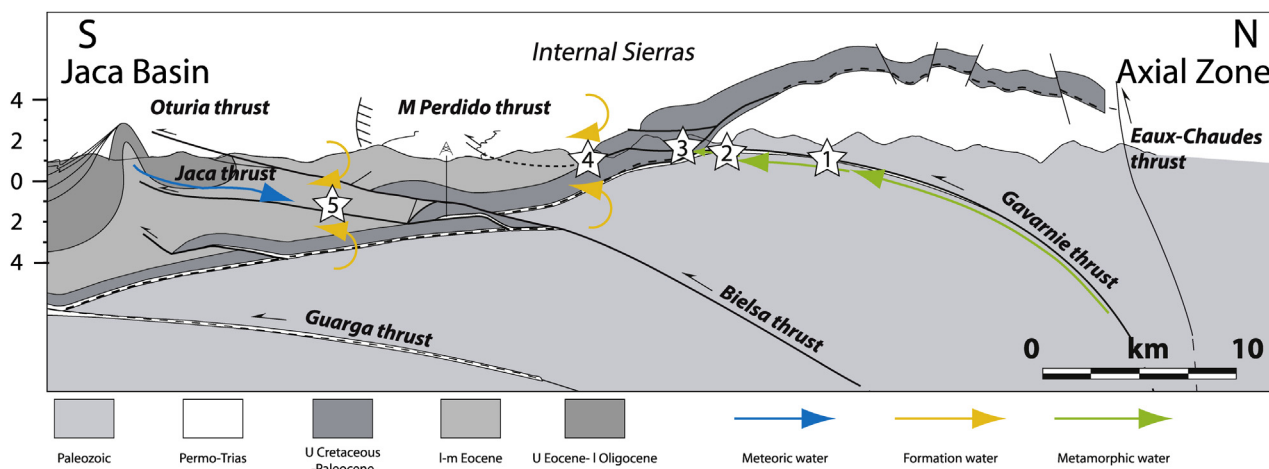


Figure 13. Conceptual model representing the different fluid sources recorded in the different fault zones discussed above. The studied localities are projected onto this reference section. Note the change in fluid sources from the hinterland (North) to the foreland (South). The cross-section is modified from Meresse (2010). Stars: Approximated location of the outcrops studied. 1: Pic de Port Vieux fault (McCaig et al., 1995); 2: Plan de Larri fault (McCaig et al., 1995); 3: Pineta thrust fault (Rye and Bradbury, 1988); 4: Monte Perdido thrust fault (Lacroix et al., 2011); 5: Jaca thrust fault (this study). Note that Castillo Mayor fault is not plotted because it is located along another cross-section more to the East.

The low fault permeability could be explained by the high clay mineral content in the fault zone, derived from the host sediments. Crawford et al. (2008) showed experimentally that permeability is negatively correlated with clay mineral contents, shear displacement and effective pressure. In the Monte Perdido thrust fault, we interpret the semi-closed fluid system as the combination of a high clay content (>60%), high shear displacement and high effective pressure during deformation.

Southward, in the inner part of the Jaca basin, this study suggests a fluid-system opening during the late stages of Jaca thrust activity (Fig. 13). We suggest that the late fluid-system opening is associated with an increase in fault permeability during the late stages of fault activity. As demonstrated by numerous studies the fabric development is closely correlated to an increase of porosity and permeability (e.g. Leclère et al., 2012 among others). During a thrust initiation, a fault formed at depth is not necessarily directly connected to the surface. During propagation of a thrust fault toward the surface, deformation within the fault core is associated with an increase in fabric development such as cleavage or shear surfaces, which could increase porosity and permeability. In the front of a thrust system, such propagation could be connected to the surface and so could trigger a percolation of surficial water from either meteoric or marine sources.

Fluid flow compartmentalization, highlighted in this study, focuses on the Gavarnie and the Monte Perdido thrust faults. The activities of both faults are not contemporaneous. Consequently, the fluid flow model presented above could be questionable. Nevertheless, focusing independently on either the Gavarnie and/or the Monte Perdido thrust faults, the same trends seem to be recorded. The results clearly highlight for both thrust faults, the contribution of metamorphic water (not re-equilibrated) in the North, marking a high fluid flow rate or low fluid-rock interactions. Southward, the hydrological fault systems are closed suggesting a high fluid-rock interactions. Finally, the frontal part of both thrust units, paleohydrological systems seems to be connected to the surface with the infiltration of surface fluids.

8. Conclusions

This study documents the high complexity of a fluid flow system in fold-and-thrust belts and suggests a structural control on fluid sources in such structures. The geochemical and petrographical analyses performed on two thrust faults and their comparison with available data on other faults, indicate a compartmentalization of the south-Pyrenean fold-and-thrust belt. In the northern part of the wedge, at the interface between the basement and first sedimentary covers, the Gavarnie-thrust and their related fault zones show the contribution of deep metamorphic water, probably from the Permo-Trias basement. In the Jaca basin, the Monte Perdido thrust fault is characterized by a closed-fluid system: such a behavior is interpreted as a consequence of high clay mineral content in the host sediments. Southwards, the Jaca and Cotiella thrust faults are characterized by a more open fluid-system, where firstly formation water and later meteoric and marine water were present.

Acknowledgments

This work was realized within the framework of the 3F “Fault, Fluid, Flow” program partially funded by INSU-CNRS and the FNS project 20020-126973/1. Isotopic analyses were realized at the University of Barcelona. We thank S. Sindern and an anonymous reviewer for constructive comments and Georgina King for English improvement.

References

- Badertscher, N.P., Beaudoin, G., Therrien, R., Burkhard, M., 2002. Glarus overthrust: a major pathway for the escape of fluids out of the Alpine orogen. *Geology* 30, 875–878.
- Beaudoin, N., Bellahsen, N., Lacombe, O., Emmanuel, L., 2011. Fracture-controlled paleohydrogeology in a basement-cored, fault-related fold: Sheep Mountain Anticline, Wyoming, United States. *Geochem. Geophys. Geosyst.* 12, Q06011.
- Beaumont, C., Muñoz, J.A., Hamilton, J., Fullsack, P., 2000. Factors controlling the Alpine evolution of the central Pyrenees inferred from a comparison of observations and geodynamical models. *J. Geophys. Res.* 105, 8121–8145.
- Bodnar, R.J., 1990. Petroleum migration in the Miocene Monterey Formation, California, USA: constraints from fluid-inclusion studies. *Mineral. Mag.* 54, 295–304.
- Boles, J.R., Eichhubl, P., Garven, G., Chen, J., 2004. Evolution of a hydrocarbon migration pathway along basin-bounding faults: evidence from fault cement. *AAPG Bull.* 88, 947–970.
- Cao, J., Jin, Z., Hu, W., Zhang, Y., Yao, S., Wang, X., Zhang, Y., Tang, Y., 2010. Improved understanding of petroleum migration history in the Hongche fault zone, northwestern Junggar Basin (northwest China): Constrained by vein-calcite fluid inclusions and trace elements. *Mar. Pet. Geol.* 27, 61–68.
- Choukroune, P., Roure, F., Pinet, B., Ecores Pyrenees Team, 1990. Main results of the ECORS Pyrenees profile. *Tectonophysics* 173, 411–423.
- Claypool, G.E., Holser, W.T., Kaplan, I.R., Sakai, H., Zak, I., 1980. The age curves of sulfur and oxygen isotopes in marine sulfate and their mutual interpretation. *Chem. Geol.* 28, 199–260.
- Craig, H., Gordon, L.L., 1965. Deuterium and oxygen-18 variations in the ocean and the marine atmosphere. In: Tongiorgi, E. (Ed.), *Proceedings of a Conference on Stable Isotopes in Oceanographic Studies and Paleotemperatures*, pp. 9–130.
- Crawford, B.R., Faulkner, D.R., Rutter, E.H., 2008. Strength, porosity, and permeability development during hydrostatic and shear loading of synthetic quartz-clay fault gouge. *J. Geophys. Res.* 113, B03207.
- Dietrich, D., McKenzie, J.A., Song, H., 1983. Origin of calcite in syntectonic veins as determined from carbon-isotope ratios. *Geology* 11, 547–551.
- Dromgoole, E.L., Walter, L.M., 1990. Iron and manganese incorporation into calcite: effects of growth kinetics, temperature and solution chemistry. *Chem. Geol.* 81, 311–336.
- Farrell, S.G., Williams, G.D., Atkinson, C.D., 1987. Constraints on the age of movement of the Montsech and Cotiella Thrusts, south central Pyrenees, Spain. *J. Geol. Soc.* 144, 907–914.
- Fitz-Diaz, E., Hudleston, P., Siebenaller, L., Kirschner, D., Camprubí, A., Tolson, G., Puig, T.P., 2011. Insights into fluid flow and water-rock interaction during deformation of carbonate sequences in the Mexican fold-thrust belt. *J. Struct. Geol.* 33, 1237–1253.
- Frezza, M.L., Tecce, F., Casagli, A., 2012. Raman spectroscopy for fluid inclusion analysis. *J. Geochem. Explor.* 112, 1–20.
- Ghisetti, F., Kirschner, D., Vezzani, L., 2000. Tectonic controls on large-scale fluid circulation in the Apennines (Italy). *J. Geochem. Explor.* 69–70, 533–537.
- Ghisetti, F., Kirschner, D.L., Vezzani, L., Agosta, F., 2001. Stable isotope evidence for contrasting paleofluid circulation in thrust faults and normal faults of the central Apennines, Italy. *J. Geophys. Res.* 106, 8811–8825.
- Goldstein, R.H., 1986. Reequilibration of fluid inclusions in low-temperature calcium-carbonate cement. *Geology* 14, 792–795.
- Goldstein, R.H., 2003. *Petrographic Analysis of Fluid Inclusions*. Mineralogical Association of Canada, pp. 9–53.
- Goldstein, R.H., Reynolds, T.J., 1994. Systematics of Fluid Inclusions in Diagenetic Minerals. SEPM short course. In: *Society for Sedimentary Geology* 31, p. 199.
- Henderson, I.H.C., McCaig, A.M., 1996. Fluid pressure and salinity variations in shear zone-related veins, central Pyrenees, France: implications for the fault-valve model. *Tectonophysics* 262, 321–348.
- Hoareau, G., Odonne, F., Debrosas, E.-J., Maillard, A., Monnin, C., Callot, P., 2009. Dolomitic concretions in the Eocene Sobrarbe delta (Spanish Pyrenees): fluid circulation above a submarine slide scar infilling. *Mar. Pet. Geol.* 26, 724–737.
- Holl, J.E., Anastasio, D.J., 1995. Cleavage development within a foreland fold and thrust belt, southern Pyrenees, Spain. *J. Struct. Geol.* 17, 357–369.
- Jolivet, M., Labaume, P., Monié, P., Brunel, M., Arnaud, N., Campani, M., 2007. Thermochronology constraints for the propagation sequence of the south Pyrenean basement thrust system (France-Spain). *Tectonics* 26, TC5007.
- Lablaume, P., Séguret, M., Seyve, C., 1985. Evolution of a turbiditic foreland basin and analogy with an accretionary prism: example of the Eocene South-Pyrenean Basin. *Tectonics* 4, 661–685.
- Lacroix, B., Buatier, M., Labaume, P., Travé, A., Dubois, M., Charpentier, D., Ventalon, S., Convert-Gaubier, D., 2011. Microtectonic and geochemical characterization of thrusting in a foreland basin: example of the South-Pyrenean orogenic wedge (Spain). *J. Struct. Geol.* 33, 1359–1377.
- Lacroix, B., Charpentier, D., Buatier, M., Vennemann, T., Labaume, P., Adatte, T., Travé, A., Dubois, M., 2012. Formation of chlorite during thrust fault reactivation. Record of fluid origin and P–T conditions in the Monte Perdido thrust fault (southern Pyrenees). *Contrib. Mineral. Petr.* 163, 1083–1102.
- Lacroix, B., Leclère, H., Buatier, M., Fabbri, O., 2013. Weakening processes in thrust faults: insights from the Monte Perdido thrust fault (southern Pyrenees, Spain). *Geofluids* 13, 56–65.
- Leclère, H., Buatier, M., Charpentier, D., Sizun, J.-P., Labaume, P., Cavailles, T., 2012. Formation of phyllosilicates in a fault zone affecting deeply buried arkosic

- sandstones: their influence on petrophysical properties (Annot sandstones, French external Alps). *Swiss J. Geosci.* 105, 299–312.
- Longstaffe, F.J., 1987. Stable Isotope Studies of Diagenetic Studies: Mineralogical Association of Canada. Mineralogical Association of Canada, Saskatoon, pp. 225–262.
- Longstaffe, F.J., Calvo, R., Ayalon, A., Donaldson, S., 2003. Stable isotope evidence for multiple fluid regimes during carbonate cementation of the Upper Tertiary Hazeva Formation, Dead Sea Graben, southern Israel. *J. Geochem. Explor.* 80, 151–170.
- McCraig, A.M., Wayne, D.M., Marshall, J.D., Banks, D., Henderson, I., 1995. Isotopic and fluid inclusion studies of fluid movement along the Gavarnie Thrust, central Pyrenees; reaction fronts in carbonate mylonites. *Am. J. Sci.* 295, 309–343.
- McCraig, A., Tritlla, J., Banks, D., 2000. Fluid mixing and recycling during Pyrenean thrusting: evidence from fluid inclusion halogen ratios. *Geochim. Cosmochim. Acta* 64, 3395–3412.
- Meresse, F., 2010. Dynamique d'un prisme orogénique intracontinental: évolution thermochronologique (traces de fission sur apatite) et tectonique de la Zone Axiale et des piedmonts des Pyrénées centro-occidentales.
- Millan Garrido, H., 2006. Estructura y cinemática del frente de cabalgamiento surpirenaico en las Sierras Exteriores aragonesa. Instituto de Estudios Altoaragoneses, p. 398.
- Muñoz, J., 1992. Evolution of a continental collision belt: ECORS-Pyrenees crustal balanced crosssection. In: *Thrust Tectonics*.
- Mutti, E., Séguret, M., Sgavetti, M., 1988. Sedimentation and deformation in the Tertiary sequences of the Southern Pyrenees. In: *Field Trip 7 Guidebook. AAPD Mediterranean Basins Conference, Nice, France. Special Publication of the Institute of Geology of the University of Parma*.
- Oliva-Urcia, B., Larrasoana, J.C., Pueyo, E.L., Gil, A., Mata, P., Parés, J.M., Schleicher, A.M., Pueyo, O., 2009. Disentangling magnetic subfabrics and their link to deformation processes in cleaved sedimentary rocks from the Internal Sierras (west central Pyrenees, Spain). *J. Struct. Geol.* 31, 163–176.
- Parry, W.T., Blamey, N.J.F., 2010. Fault fluid composition from fluid inclusion measurements, Laramide age Uinta thrust fault, Utah. *Chem. Geol.* 278, 105–119.
- Puigdefabregas, C., 1975. La sedimentación molásica en la cuenca de Jaca. In: *Monografías Instituto Estudios Pirenaicos* 104, p. 188.
- Roedder, E., 1984. Fluid Inclusions. *Reviews in Mineralogy*. In: *Reviews in Mineralogy* 12.
- Rye, D.M., Bradbury, H.J., 1988. Fluid flow in the crust; an example from a Pyrenean thrust ramp. *Am. J. Sci.* 288, 197–235.
- Séguret, M., 1972. Etude tectonique des nappes de séries décollées de la partie centrale du versant sud des Pyrénées. Caractère synsédimentaire, rôle de la compression et de la gravité (Thèse de doctorat).
- Sharp, Z.D., 2009. Application of Stable Isotope Geochemistry to Low-grade Metamorphic Rocks. Blackwell Publishing Ltd.
- Sterner, S.M., Bodnar, R.J., 1984. Synthetic fluid inclusions in natural quartz I. Compositional types synthesized and applications to experimental geochemistry. *Geochim. Cosmochim. Acta* 48, 2659–2668.
- Teixell, A., 1996. The Anso transect of the southern Pyrenees: basement and cover thrust geometries. *J. Geol. Soc.* 153, 301–310.
- Teixell, A., 1998. Crustal structure and orogenic material budget in the west central Pyrenees. *Tectonics* 17, 395–406.
- Teixell, A., Garcia-Sansegundo, J., 1996. Estructura del sector central de la Cuenca de Jaca (Pirineo central). *Rev. Soc. Geol. Esp.* 8, 207–220.
- Travé, A., Labaume, P., Calvet, F., Soler, A., 1997. Sediment dewatering and pore fluid migration along thrust faults in a foreland basin inferred from isotopic and elemental geochemical analyses (Eocene southern Pyrenees, Spain). *Tectonophysics* 282, 375–398.
- Travé, A., Labaume, P., Calvet, F., Soler, A., Tritlla, J., Buatier, M., Potdevin, J.-L., Séguret, M., Raynaud, S., Briquieu, L., 1998. Fluid Migration During Eocene Thrust Emplacement in the South Pyrenean Foreland Basin (Spain): an Integrated Structural, Mineralogical and Geochemical Approach. In: *Geological Society, London, Special Publications* 134, pp. 163–188.
- Travé, A., Labaume, P., Vergés, J., 2007. Fluid systems in foreland fold-and-thrust belts: an overview from the Southern Pyrenees. In: *Thrust Belts and Foreland Basins. Frontiers in Earth Sciences. Springer Berlin Heidelberg*, pp. 93–115.
- Verlaguet, A., Goffé, B., Brunet, F., Poinssot, C., Vidal, O., Findling, N., Menut, D., 2011. Metamorphic veining and mass transfer in a chemically closed system: a case study in Alpine metabauxites (western Vanoise). *J. Metamorph. Geol.* 29, 275–300.
- Wiltschko, D.V., Lambert, G.R., Lamb, W., 2009. Conditions during syntectonic vein formation in the footwall of the Absaroka Thrust Fault, Idaho-Wyoming-Utah fold and thrust belt. *J. Struct. Geol.* 31, 1039–1057.
- Wogelius, R.A., Fraser, D.G., Wall, G.R.T., Grime, G.W., 1997. Trace element and isotopic zonation in vein calcite from the Mendip Hills, UK, with spatial-process correlation analysis. *Geochim. Cosmochim. Acta* 61, 2037–2051.
- Zheng, Y.F., 1999. Oxygen isotope fractionation in carbonate and sulfate minerals. *Geochem. J.* 33, 109–126.